Available online at www.sciencedirect.com

jmr&t
Journal of Materials Research and Technology
www.jmrt.com.br

Original Article

Process mineralogy of rare earths from deeply weathered alkali-carbonatite deposits in Brazil

Juliana Lívi Antoniassi, Daniel Uliana, Renato Contessotto, Henrique Kahn, Carina Ulsen*

Universidade de São Paulo, Mining and Petroleum Engineering Department, Technological Characterization Laboratory (LCT-USP), Av. Prof. Mello Moraes, 2373, 05508-030 Sao Paulo, SP, Brazil

ARTICLE INFO

Article history:
Received 31 March 2020
Accepted 31 May 2020
Available online 23 June 2020

Keywords:
Rare earth elements
Monazite
Bastnaesite
Brazilian deposits
Process mineralogy

ABSTRACT

Brazil has the second largest rare earths mineral (REM) resource in the world, mainly associated with the weathered portion of carbonatite complexes. This paper reports process mineralogy studies performed for 10 samples collected from the deeply weathered portion of different relevant Brazilian deposits, having a soil appearance and varied grain sizes with a significant content of natural fines (below 20 μm). The results indicate that REM are mainly composed of light rare earth elements and present a fine-grained nature and intricate associations with gangue minerals. Monazite is by far the most relevant REM; cerianite and bastnaesite are typical of only one of the studied deposits. The complexity of the occurrence of the rare earths challenges the development of mineral processing routes. A scandium phosphate mineral identified as a trace in one of the studied deposits has not yet been reported in the Brazilian alkaline complexes.

1. Introduction

Considerable attention has been paid to rare earth mineral (REM) resources over the last decade. The demand for rare earth elements (REEs: lanthanides – La to Lu, scandium – Sc, and yttrium – Y) in high technology applications has increased, and because China accounts for about 70% of world production [1,2], the search for new resources has intensified in several countries [3,4].

The policies of the Brazilian government have encouraged the exploration of new REE projects under the 2030 National Mining Plan for strategic minerals. Financial support is provided for R&D in the entire REE production chain to overcome technological issues in exploiting Brazilian REE resources [5–8].

Brazil was the major producer of REEs from the late 19th until the early 20th century, from the monazite-rich sand deposits of the Bahia State coast [9]. Currently, this production is interrupted due to restrictions related to thorium and uranium contents and only the available concentrates in stock are being sold [7]. However, recent data indicate that Brazil, together with Vietnam, hosts the second largest global resources of mainly light REEs (LREEs) (22 million tons; [2,10]),

* *Corresponding author.*
E-mail: juliana@lct-usp.org (J.L. Antoniassi).
https://doi.org/10.1016/j.jmrt.2020.05.128

Table 1 – Chemical composition and size fractions distribution (%) (bulk samples).

Samples	A1	A2	A3	A4	A5	B1	B2	C1	D1	D2
ICP (REO; ppm)										
La_2O_3	5960	8558	3187	10686	4938	2785	3372	9178	8530	14684
CeO_2	11408	16086	5645	19513	12444	5816	7167	23223	19113	32810
Pr_6O_{11}	1152	1667	646	1927	1422	667	721	1577	1912	3349
Nd_2O_3	3786	5699	2660	6835	4858	2155	2641	4751	6348	10766
Sm_2O_3	744	1039	625	1448	1018	438	439	810	1286	1346
Eu_2O_3	176	251	149	347	188	106	110	186	267	212
Gd_2O_3	387	537	324	834	315	218	230	352	501	429
Tb_4O_7	53	71	53	139	53	32	39	75	84	76
Dy_2O_3	187	244	186	497	117	100	110	184	184	140
Ho_2O_3	24	32	26	82	20	<5	<5	32	10	14
Er_2O_3	63	81	65	169	31	34	38	57	44	31
Tm_2O_3	6	6	6	20	<5	<5	<5	<5	<5	<5
Yb_2O_3	26	32	46	99	25	6	10	48	24	10
Lu_2O_3	<5	<5	<5	9	<5	<5	<5	5	<5	<5
Sc_2O_3	272	352	247	435	377	96	216	8	242	238
Y_2O_3	683	981	824	2210	354	275	331	461	615	395
Total ($\sum$REO)	24925	35637	14693	45252	26164	12730	15425	40952	39164	64501
XRF (Major oxides; wt%)										
MgO	0.45	0.28	0.25	0.18	0.22	1.33	2.2	0.23	0.39	0.32
Al_2O_3	7.86	8.46	22.2	12.5	23.7	3.54	4.62	24.1	3.32	2.73
SiO_2	4.9	20.8	37.3	11.6	23.7	15.6	6.3	24	15.2	22
P_2O_5	6.72	8.17	2.34	8.27	3.32	1.36	4.32	0.51	6.96	9.53
K_2O	<0.10	0.12	0.76	<0.10	0.46	<0.10	<0.10	2.6	0.11	0.1
CaO	1.15	1.34	0.14	0.33	0.15	4.71	2.35	0.14	2.69	5.6
TiO_2	8.23	9.22	2.3	3.73	2.9	30.3	25.3	2.53	12.7	8.25
MnO	1.58	1.11	0.84	2.65	1.62	0.53	1.07	2.76	1.25	0.99
Fe_2O_3	49.2	31.1	20.4	37.3	25.7	35.8	44.2	26.6	43.4	36.1
SrO	0.64	0.9	0.26	0.96	0.25	0.12	0.38	<0.10	0.55	0.59
ZrO_2	0.31	0.3	0.14	0.32	0.23	0.1	0.15	0.38	0.72	0.35
Nb_2O_5	0.51	0.53	0.33	0.76	0.19	0.19	0.43	0.17	0.36	0.36
BaO	4.49	4.68	1.3	5.22	2.17	<0.10	0.2	0.1	2.03	1.8
ThO_2	<0.10	<0.10	<0.10	0.13	<0.10	<0.10	<0.10	0.73	<0.10	<0.01
U_3O_8	<0.10	<0.10	<0.10	<0.10	<0.10	<0.10	<0.10	<0.10	<0.10	<0.10
LOI	11	10.1	10.5	10.6	12.8	5.71	7.26	10.2	5.31	4.63
Total	97	97.1	99.1	94.6	97.4	99.3	98.8	95.1	95	93.3
Sieve size analysis										
wt distribution (%)										
+0.30 mm	17.3	16.3	10.2	16.4	13.4	38.3	27.2	27.7	29.4	49
-0.30+0.074 mm	22.7	22.7	11.8	11.6	9.4	26.8	26.5	10.8	21.4	13.2
-0.074+0.020 mm	20.2	21	13.7	13.3	13	13	17.5	10.7	21.6	10.6
-0.020 mm - underflow	21.9	19.5	17.3	19.7	17.3	10.5	12.3	27.2	13.2	13.2
-0.020 mm - overflow	17.8	20.5	47.1	39	46.9	11.3	16.5	23.5	14.3	14.1
REO distribution (%)										
+0.30 mm	8.0	9	8.6	6.6	16.8	31.3	17.9	36.9	14.6	22.3
-0.30+0.074 mm	13.3	13.5	7.7	6	10.3	20.9	18.6	16.6	10.1	5.9
-0.074+0.020 mm	19.0	18.8	10.9	11.3	13.7	12.4	18.2	13.1	15.7	7.7
-0.020 mm - underflow	32.4	27.5	20.8	25.7	17.5	16.3	20	20.1	21.6	27.9
-0.020 mm - overflow	27.4	31.2	52	50.5	41.7	19.2	25.3	13.3	38	36.1

which are mostly associated with carbonatite complexes [11]. This large volume of Brazilian resources helps to drive the R&D activities for the REE production chain in the country.

Process mineralogy studies applied to REE mineralization in the Brazilian carbonatites are poorly documented in the literature. Tassinari et al. [12] and Neumann and Valarelli [13] initially investigated the mineralogical complexity associated with the Catalão complex, where REMs mainly occur as fine-grained monazite with complex associations with gangue minerals. Physical separation techniques including density methods, magnetic separations, and even flotation have not yielded satisfactory results. Recent mineralogical studies for specific deposits using advanced characterization techniques show the complexity of the ores and difficulty in concentrating the REMs by physical separation [14–17].

This study reports the chemical and mineralogical features of REMs from a set of 10 samples from the four major Brazilian occurrences of rare earths as well as the implications for mineral processing. The purpose of the paper is to contribute to current knowledge by providing a detailed characterization of REM occurrences and associations to face physical concentration or even hydrometallurgical extractions which may be a possible alternative for processing these resources.

2. Materials and methods

2.1. Samples and experimental procedures

The study was carried out in 10 representative samples from four major Brazilian alkaline carbonatite deposits – Barreiro, Salitre, Morro do Ferro, and Catalão – located in the States of Minas Gerais and Goiás. Samples were identified as deposit A (five samples, A1 to A5, collected in different and representative areas of the deposit), B (two samples, B1 and B2), C (one sample, C1), and D (two samples, D1 and D2), respectively.

Samples were collected from the deeply weathered areas of the carbonatites, having a soil appearance and varied grain sizes with a significant content of natural fines (below 0.020 mm). The experimental procedure adopted for the mineralogical characterization of each sample comprised:

- homogenization and sampling of the bulk sample;
- initial sieve size analysis by wet screening with screen apertures of 0.30, 0.074, and 0.020 mm; the material below 0.020 mm was also deslimed in a 25-mm-diameter hydrocyclone with a cut size of around 7 μm;
- chemical analyses of the bulk sample and all size fractions by X-ray fluorescence (XRF) and inductively coupled plasma optical emission spectroscopy (ICP-OES);
- identification of the major mineral associations by scanning electron microscopy (SEM) and definition of the comminution size (P95–95% w/w passing through) based on the mineral grain sizes and their associations;
- selected samples (A1, A2, B1, B2, C1, D1, D2) were ground below 0.30 or 0.125 mm in a rod mill; samples A3, A4, and A5 were not ground due to their original proportion of fines below 0.020 mm;
- all samples were submitted to another sieve size analysis by wet screening (screen apertures of 0.30, 0.15, 0.074, and 0.020 mm) and desliming by hydrocyclone (predicted size below 7 μm) to perform the detailed mineralogical studies by automated X-ray based image analysis with X-ray diffraction (XRD) support.

2.2. Analytical methods

2.2.1. Chemical analysis

The REEs in bulk samples were quantified by ICP-OES (Horiba Ultima Expert) after performing the four-acid digestion method. Loss on ignition (LOI) was performed by sample calcination in a muffle furnace at 1050 °C for 1 h. Routine quantitative analyses were carried out by XRF in fused beads to determine the major oxides above 0.10 wt% in an S8 Tiger spectrometer (Bruker AXS).

2.2.2. XRD

Mineralogical analysis was performed by XRD using the powder method with Cukα radiation (D8 Endeavor diffractometer, from Bruker AXS), and the mineral quantification utilized the Rietveld refinement method (using Topas software and database).

2.2.3. SEM-based automated mineralogy

The modal mineralogy, elemental distribution of the main oxides in the bearing minerals, and mineral associations by area and perimeter of contact were determined by sieve fraction, with an automated image analysis system (MLA software, FEI) coupled with an FEI Quanta 650 FEG SEM coupled to an energy dispersive spectrometer (EDS–Esprit, Bruker Nano Analytics). This technique is considered very robust and has been widely used in the mining industry for quantitative mineralogical studies including studies of REE resources [14,16,18–20]. The analyses were performed considering both the atomic number contrast [backscattered electron (BSE) images] and the chemical composition of each mineral species (characteristic X-ray spectra by EDS) – XBSE mode. The chemical composition of each mineral was determined using a LEO Stereoscan 440 SEM with an EDS detector (INCA x-act, Oxford) calibrated with certified reference standards. The operating conditions made possible the identification of REM grains with sizes down to 5 μm (pixel size of 1 μm).

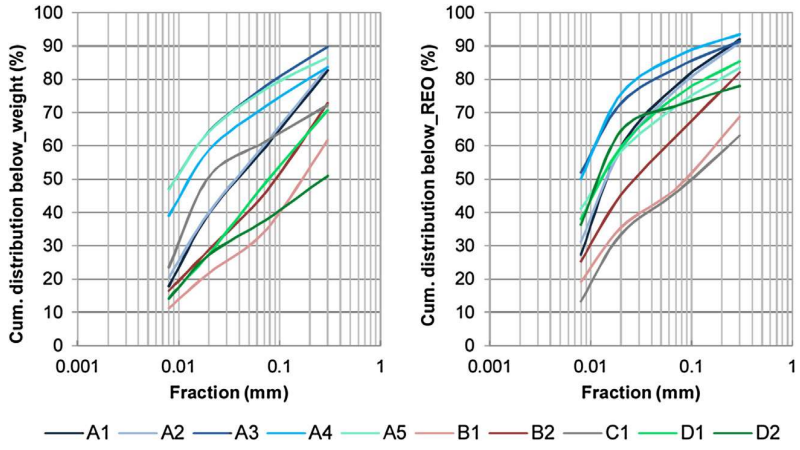

Fig. 1 – Cumulative weight and REO distributions (bulk samples).

3. Results and discussion

3.1. *Chemical composition and distribution by size fractions*

The chemical composition of bulk samples [highlighting the sum of the rare earth oxides (REOs)] as well as the mass and REO distributions by sieve fraction is presented in Table 1.

The REO content ranges from 1.27 to 6.45 wt% (12,730–64,501 ppm) in the studied samples, which are mainly composed of LREEs such as CeO_2, La_2O_3, Nd_2O_3, Pr_6O_{11}, and Sm_2O_3. These grades are common in the Brazilian carbonatite complexes [9–11]. The CeO_2 content represents about 50% of the total REOs in these deposits, while Nd_2O_3 (which has high commercial value together with praseodymium [21]) rarely exceeds the La_2O_3 content (e.g. sample A5). Heavy rare earth element (HREE) concentrations (including Y_2O_3 and Sc_2O_3 contents) are low and represent around 6–8% of the total REOs in deposits A and B and 3% in deposits C and D. The bulk of the mass consists of varied proportions of significant Fe_2O_3, SiO_2, and Al_2O_3, and lesser amounts – although possibly of economic importance – of BaO, TiO_2, P_2O_5, and Nb_2O_5 [11,22,23]. Critical contents such as thorium and uranium are low and generally less than 0.01% in the samples, even those from Morro do Ferro deposit, which is known due the radioactive elements enrichments in some weathering zones [24].

The sieve size classification indicates significant weight proportions of particles below 20 μm, which contain most of the REEs in the samples (greater than 60% of the REOs in deposits A and D; Fig. 1 – cumulative undersize distributions) in agreement with other studies [12,13,16] with notably high content in the slime fraction (overflow product with predicted size below 7 μm). Some samples also have a considerable mass proportion of coarser material: an average of 35 wt% is coarser than 0.30 mm in samples B, C, and D and accounts for around 25% of the total REOs.

3.2. *Mineralogical composition and the rare earth minerals (ground or bulk samples)*

The mineralogical composition of samples is represented in Fig. 2(a) and reflects both metasomatic mineralization and the later supergenic enrichments by the extreme lateritic physical-chemical weathering of carbonatite bodies. Some primary minerals, such as carbonates and apatite, are usually transformed while less mobile elements and resistant minerals are retained [1,11,23,25].

The mineral assemblage is composed of Fe-oxy-hydroxides (goethite, hematite, and rarely magnetite), Al-phosphates (plumbogummite-group minerals), fluorapatite, quartz, kaolinite, gibbsite, micaceous minerals (biotite, phlogopite, vermiculite, and interlayered clay minerals), ilmenite, anatase, and perovskite. The typical REMs include monazite [(REE)PO_4], bastnaesite [(REE)(CO_3)F], cerianite (CeO_2), traces of xenotime

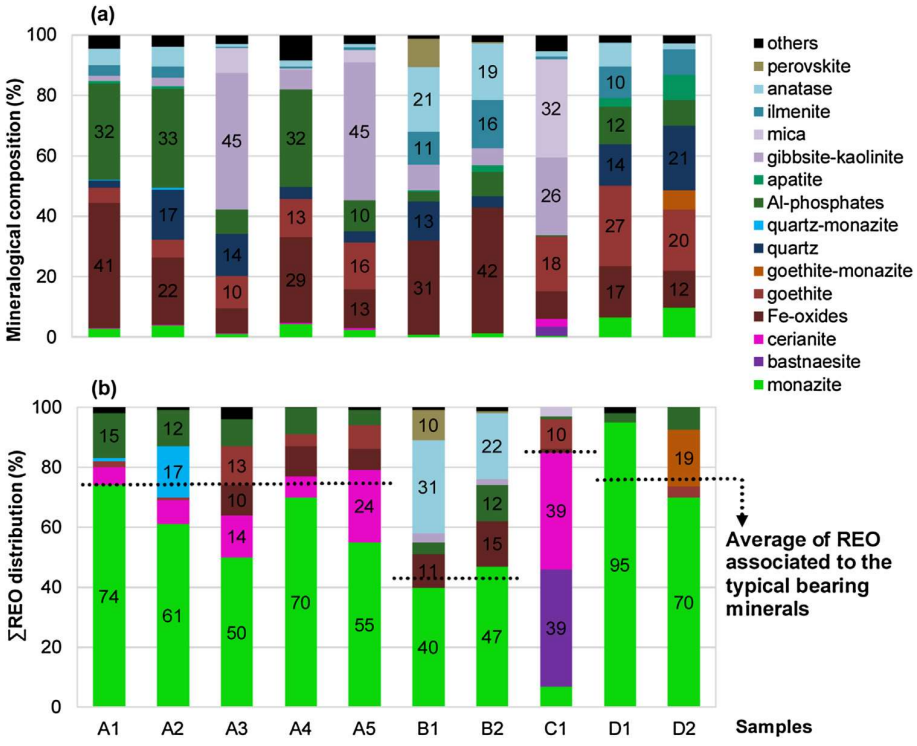

Fig. 2 – Mineralogical composition of bulk samples (a; wt%) and the REO distribution among REE-bearing minerals (b; %) (MLA/EDS software).

Table 2 – Rare earth minerals (wt.%) by sieve size fraction at different comminution top sizes (X-ray based image analysis).

	Samples									
	A1	A2	A3	A4	A5	B1	B2	C1	D1	D2
Top size (mm) Comminution (P95)	−0.30	−0.30	bulk	bulk	bulk	−0.30	−0.30	−0.125	−0.30	−0.30
Monazite (wt.%)										
+0.30 mm			0.4	0.8	2.1					
−0.30 + 0.15 mm	1.0	1.7	0.4	1.2	2.4	0.3	0.6		2.1	4.6
−0.15 + 0.074 mm	1.6	2.2	0.6	2.2	3.1	0.5	1.0	0.4	2.6	4.8
−0.074 + 0.020 mm	2.0	3.6	0.6	4.0	2.8	0.7	1.2	0.6	4.7	9.9
−0.020 mm – underflow	4.5	6.4	1.4	5.4	2.5	1.2	1.4	0.7	9.4	15
−0.020 mm – overflow*	5.6	5.9	1.5	5.6	2.2	2.5	2.4	0.4	16	17
REMs (monazite + bastnaesite + cerianite + xenotime + Sc-phosphate; wt.%)										
+0.30 mm				0.9	3.8					
−0.30 + 0.15 mm	1.1	1.9	0.6	1.4	3.5	0.3	0.6		2.1	4.6
−0.15 + 0.074 mm	1.8	2.5	0.8	2.6	3.7	0.5	1.0	8.0	2.6	4.8
−0.074 + 0.020 mm	2.2	4.1	0.8	4.4	3.5	0.7	1.2	8.9	4.7	9.9
−0.020 mm – underflow	4.8	6.8	1.6	5.8	3.1	1.2	1.4	6.3	9.4	15
−0.020 mm – overflow*	5.8	6.1	1.5	5.7	2.5	2.5	2.4	3.2	16	17

* Note: minerals may be slightly underestimated in the image analysis due to the pixel size resolution; for this reason, mineralogical proportions were also performed by the XRD-Rietveld refinement method.

(YPO_4), and probably pretulite ($ScPO_4$). Accessory minerals include carbonates, zircon, calzirtite, zirkelite–zirconolite, baddeleyite, barite, BaMn-oxy-hydroxides, Ba and Pb-rich pyrochlore group minerals, feldspars, pyroxene, pyrite, titanite, thorianite, Th-phosphate, Cr-spinel, and priderite.

Regarding the REEs (Fig. 2(b)), monazite is the main bearing mineral, except for deposit C, which is enriched in bastnaesite and cerianite. Other rare earth bearing minerals commonly found in carbonatite laterites, such as cerite, parisite, and synchysite [23], were not identified. Scandium phosphate occurs in trace quantities in deposit A and its occurrence is not documented in Brazilian deposits; scandium has the highest added value among the REEs, with prices exceeding more than hundred times those of other LREEs [21].

Table 2 summarizes the grinding conditions and the grades of REMs by size fraction. The grades of REMs increase toward the finer fractions (except for samples A5 and C1), which is reflected in the chemical analyses by size fraction. As an example, the proportion of REMs in the overflow product reaches 17 wt% in sample D2 (25 wt% if calculated by XRD-Rietveld, Fig. 3) for the adopted grinding condition (below 0.30 mm).

The REO distribution in Fig. 2(b) shows that monazite, bastnaesite, and cerianite account for most of the REEs in samples, ranging from around 80% in deposits A, C, and D to 43% in B.

Therefore, a considerable portion of the REOs are associated with other minerals beyond the typical carriers. This is attributed to the deposit's genetic formation processes, when different minerals incorporate REEs during the supergenic evolution [24,26–29], and is also related to the occurrence of undetectable submicron inclusions of REE-bearing minerals associated with other minerals, particularly with iron hydroxides-oxides and quartz.

Depending on the size of these associations and the pixel size in the image analysis by MLA/SEM (REE-bearing minerals versus host minerals), it is sometimes impossible to perform a proper mineral classification considering workable resolution criteria [15,16,19]. Thus, the host minerals are assumed to contain a part of the rare earths present (tiny inclusions), whereas the proportions of typical REMs may be slightly underestimated (especially in the finer size fractions). This can be illustrated with the so-called goethite–monazite phase classified in sample D2 as an intimate and indistinguishable association between these two minerals, as well as the quartz–monazite in sample A2. Other minerals incorporating REE contents are mainly Al-phosphates (up to 5% of REOs) for most samples and anatase (up to 3% of REOs) essentially in deposit B.

The reliability of the reported data was verified considering the reconciliation of the chemical results assayed by XRF against those calculated by MLA based on modal mineralogy (Fig. 4).

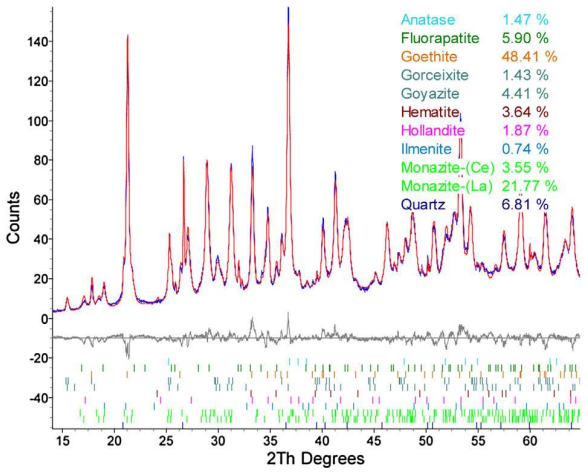

Fig. 3 – XRD-Rietveld analyses applied to the D2 sample – overflow product.

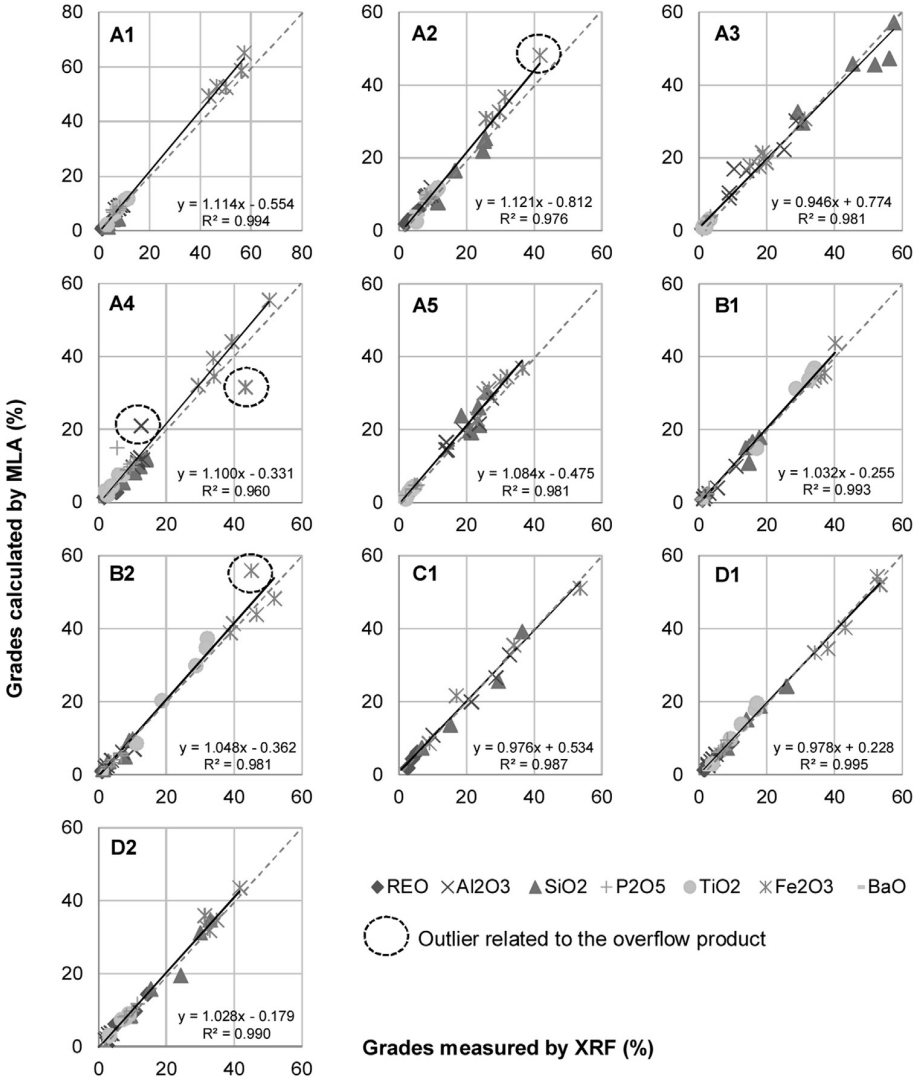

Fig. 4 – Comparison of sample bulk chemistry calculated by MLA and measured by XRF.

3.3. *Characteristics of REM: chemistry and physical aspects*

A summary of the chemical composition of REMs obtained by the microanalysis system (SEM-EDS) is shown in Table 3. Monazite crystals show considerable compositional variability; the predominant variety is rich in cerium, although lanthanum and/or neodymium enrichment is also common, all usually occurring as intergrowth variations. Scandium and some other HREEs are sporadically observed in monazite, always in low concentrations, close to the limit of the EDS detection. Micro-crystallinity, porosity, and the possibility of hydration are factors that can interfere with the sensitivity of EDS analyses as these analyses are often hampered by the proximity of the REE emission lines [30].

The compositional variability of bastnaesite is reflected in the cerium and lanthanum concentrations; thorium is usually present in higher proportions than in monazite, while yttrium occurs rarely, as a trace. Cerianite is composed essentially of cerium, showing varieties rich in thorium or iron (maximum of 10 wt%). Among the trace minerals (observed essentially in deposit A), xenotime contains predominantly yttrium with traces of samarium, gadolinium, dysprosium, holmium, and erbium (HREEs), while Sc-phosphate has practically no compositional variation.

The main chemical and physical features observed by SEM/EDS/MLA for the typical REE-bearing minerals are illustrated in terms of morphology (Fig. 5), chemical composition (EDS analysis, Fig. 6), associations (Fig. 7), and grain size (Fig. 8). In common, REMs from the studied deposits are characterized by micrometric grain size and occur as aggregates with

Table 3 – REE chemical varieties in the bearing minerals (average weight percentage and non- normalized results; SEM-EDS).

Mineral	La_2O_3	CeO_2	Pr_6O_{11}	Nd_2O_3	Sc_2O_3	Y_2O-$_3$	ThO_2	P_2O_5
Monazite-(Ce)	14.4	30.4	1.13	8.36	tr		0.33	27.9
Monazite- (CeLaNd)	15.1	22.6	3.79	15.5	tr		1.64	26.8
Monazite-(La)	29.3	14.3	tr	7.06			tr	30.0
Monazite-(Nd)	13.8	8.42	4.89	27.2			1.17	27.4
Other constituents: REO, H_2O; tr = SiO_2, Al_2O_3, Fe_2O_3, CaO, SrO, BaO								
Bastnaesite-(Ce)	15.3	29.4	tr	6.37			5.95	0.22
Bastnaesite- (CeLa)	21.8	17.4	2.50	11.3		tr	4.63	0.58
Other constituents: REO, F, CO_2; tr = SiO_2, Al_2O_3, Fe_2O_3, CaO								tr
Cerianite-(Ce)	tr	90.3	tr	tr	tr		0.86	2.61
Cerianite-(CeTh)	tr	80.8	tr	tr	tr		10.1	1.70
tr = REO, SiO_2, Al_2O_3, Fe_2O_3, MnO, TiO_2, Nb_2O_5, U_3O_8								
Xenotime						49.3	4.89	25.9
tr = REO, SiO_2, Fe_2O_3, CaO, U_3O_8								
Sc-phosphate					44.9			51.3
tr = Al_2O_3, Fe_2O_3								

Note: tr = trace contents..

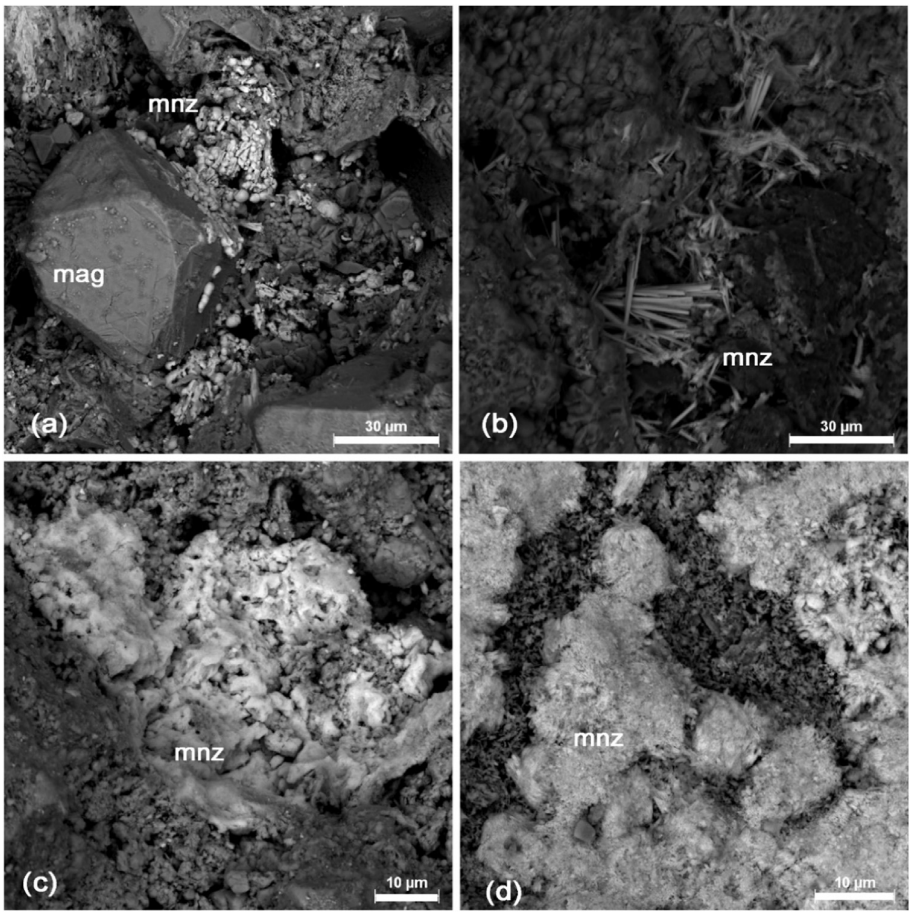

Fig. 5 – SEM-BSE images. Aspects of monazite crystals: colloform (a), acicular (b), massive (c), and as micrometric aggregates (d), usually porous and related to the intergrowth of REE minerals. Mnz = monazite; Mag = magnetite.

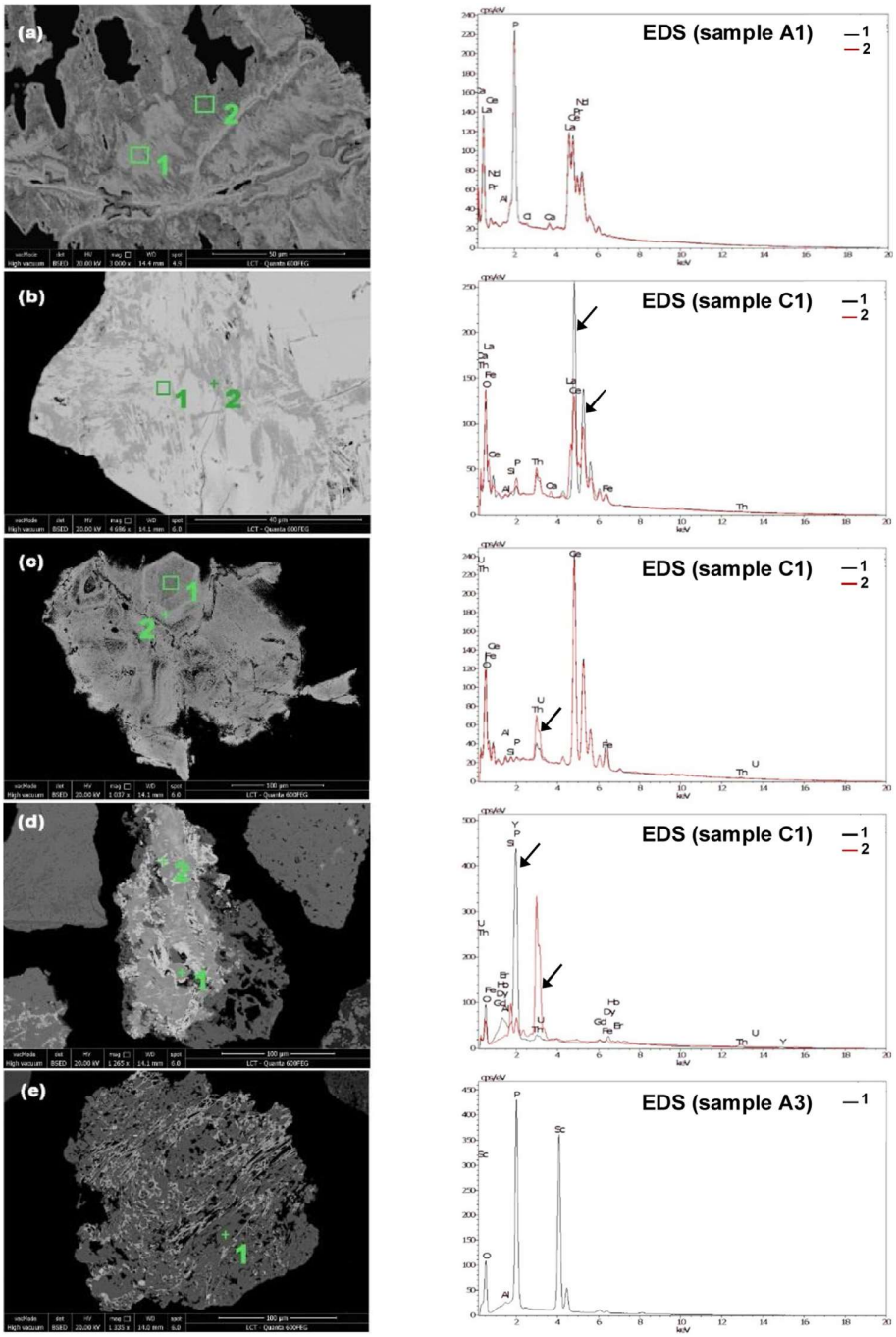

Fig. 6 – SEM-EDS analysis. Typical REE minerals. Compositional variability (hydration) in monazite (a) and related to the Ce–La contents in bastnaesite (b). Free porous cerianite (liberated), exhibiting Th zoning (c). Complex intergrowth association between xenotime and thorianite (d). Sc-phosphate mixed with goethite (e).

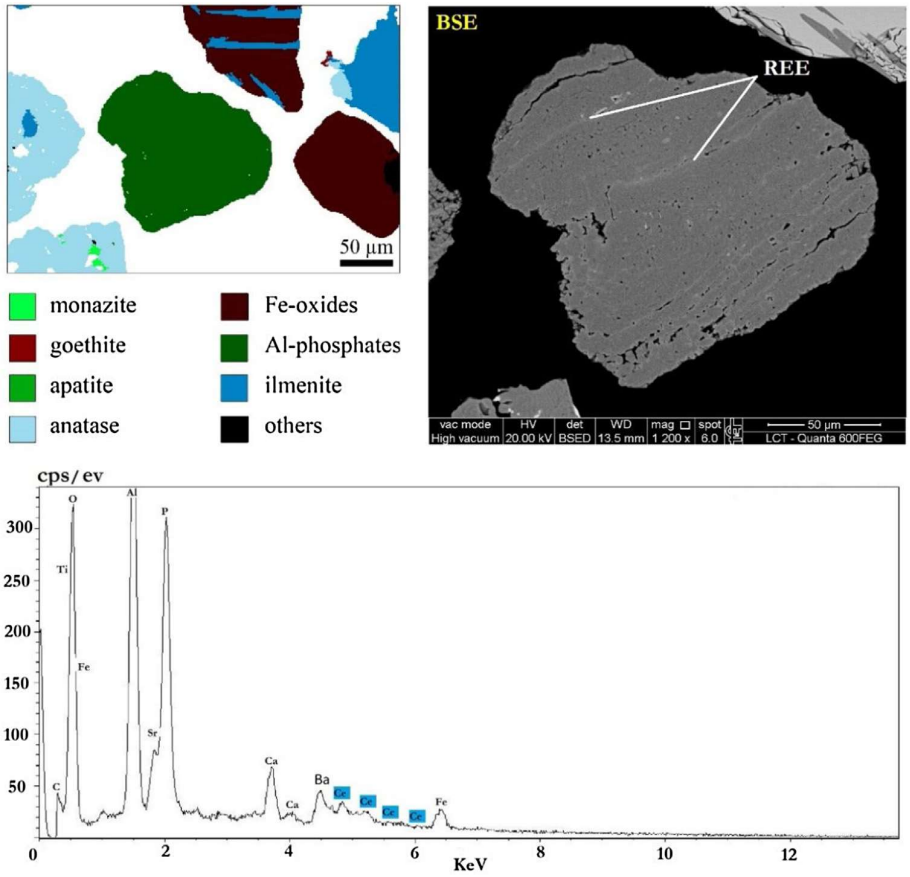

Fig. 7 – Free Al-phosphate particle (liberated) classified by MLA image analysis. Presence of tiny veins enriched in an REE-bearing phase on the EDS spectrum (below MLA/SEM image analysis resolution) (modified from [15]).

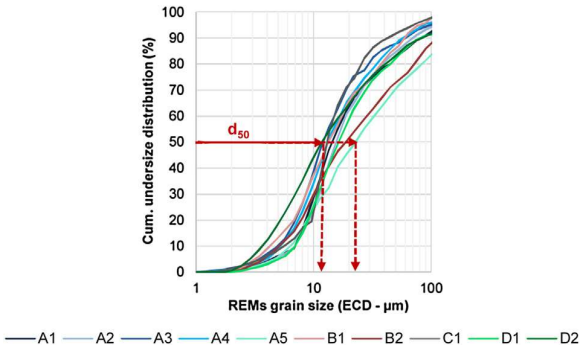

Fig. 8 – Size distribution of rare earth minerals and aggregates.

a porous aspect and average size [equivalent circle diameter (ECD)] from 12 to 22 µm (for the material above 7 µm).

3.4. *Rare earth minerals associations*

The typical associations of REMs and their aggregates reach an average degree of liberation of around 50 wt% by area (Fig. 9(a)); free particles are those composed by more than 95% REMs.

The degree of liberation by area increases gradually toward the fines, occurring incompletely even at very fine-grained stages due to intergrowths with other minerals [14], or just indistinguishable at the resolution adopted for the image analysis. Samples A1 and D1 reach a degree of liberation of 67% by area in the −0.074 + 0.020 mm fraction; however, in the other samples, values higher than 60% are observed only in the fraction below 0.020 mm (Fig. 9(b)).

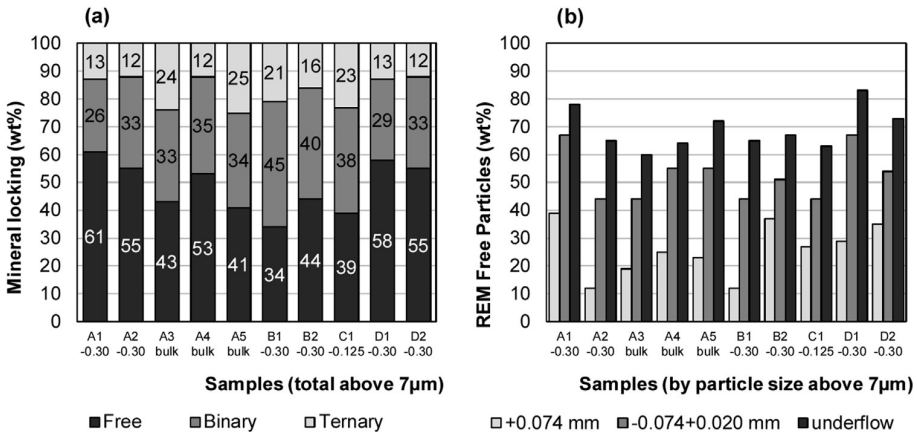

Fig. 9 – Occurrence of rare earth minerals (a) and frequency of free particles by particle size (b).

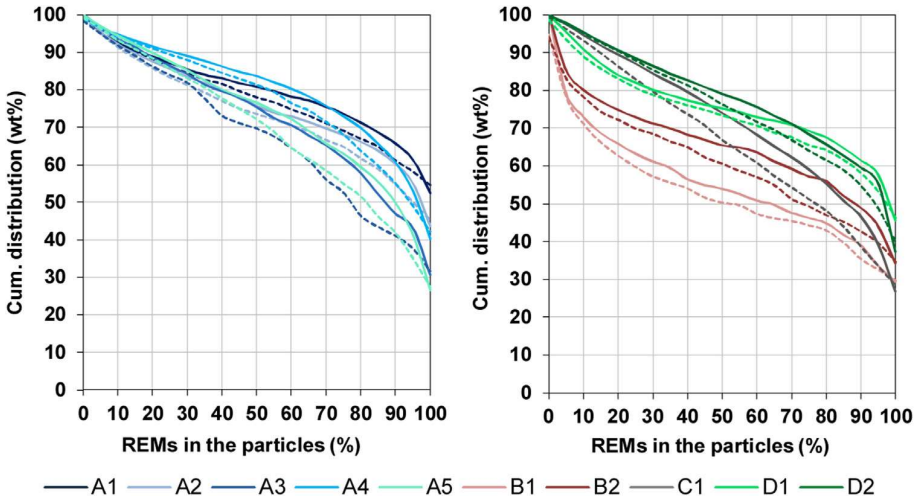

Fig. 10 – Comparison between the degree of liberation of rare earth minerals by area (solid line) and perimeter of contact (dashed line) (total analyzed above 7 μm).

The degree of liberation by perimeter of contact is slightly lower than that by area due to the tendency of the gangue minerals to concentrate at the border of locked particles (Fig. 10). In locked particles, the REMs usually occur as micro-inclusions, mostly associated with Al-phosphates, Fe-oxy-hydroxides, anatase (essentially in deposit B), mica (essentially in deposit C), BaMn-oxy-hydroxides, and quartz (Table 4).

4. Conclusions

The studied deposits show particularities in terms of chemical and modal mineralogical composition typically related to the genetic and lateritic differentiations of Brazilian alkaline–carbonatite complexes. However, the 10 studied samples show the complexity of REO occurrence and mineral associations with the gangue.

Relevant features observed for the REMs are:

- *REMs:* monazite, bastnaesite and cerianite account for an average of 70% of the total REOs in samples; xenotime and scandium phosphate are traces.
- *Chemical variability:* this is more evident for the proportions of cerium and lanthanum (the main REEs contained); the ThO_2 content when present varies from 1% to 4% in the monazite and 1% to 9% in the bastnaesite and generally reaches 10% in the cerianite.
- *Reduced grain sizes:* d_{50} from 12 to 22 μm for the material above 7 μm; REMs commonly occur as microcrystalline aggregates (intergrowth of REMs) with high porosity.
- *Low degree of liberation:* in general, this reaches only 60% in the ultrafine fractions (below 20 μm).

The low degree of liberation and occurrence in ultrafine-grained REE-bearing minerals are a challenge for the development of mineral processing routes since existing technologies are limited for those features. The energy for grinding of this fraction could be evaluated as well as mag-

Table 4 – Mineral locking for all rare earth minerals (wt.%; total + 7 μm). The main gangue minerals associated with the rare earth minerals (binary and more complex associations) are highlighted in bold.

Samples	A1	A2	A3	A4	A5	B1	B2	C1	D1	D2
Topsize (mm)	0.30	0.30	1.19	1.19	1.19	0.30	0.30	0.125	0.30	0.30
wt.% retained in 7 μm	75.9	77.1	52.9	61.0	53.1	83.0	78.6	66.1	82.1	82.8
Mineral locking (%)										
Free	63	56	43	53	41	32	44	41	58	55
Binary	24	27	33	35	34	45	39	38	29	33
Other associations	13	17	24	12	25	23	17	21	13	12
Binary association (%)										
Fe-oxides	**2.9**	1.8	**13**	**15**	**17**	0.6	1.7	1.0	0.6	0.5
Goethite	**7.8**	**5.6**	3.1	2.2	2.6	**8.1**	**16**	**19**	**11**	**12**
Quartz	0.3	**6.4**	0.4	1.5	0.2	1.9	0.9	**–**	3.1	**13**
Al-phosphates	**8.4**	**8.1**	**6.4**	**8.3**	**3.5**	4.4	**4.3**	0.3	**3.5**	**2.4**
Apatite	0.1	0.1	–	–	–	0.1	0.2	**–**	0.1	1.7
Gibbsite + kaolinite	0.4	0.1	2.3	0.3	1.4	0.5	0.3	2.6	–	–
Micas	<0.1	<0.1	<0.1	0.1	0.2	–	–	**6.2**	–	–
Ilmenite	0.5	0.6	0.1	0.1	<0.1	3.5	1.9	0.4	1.0	0.9
Ti-oxides	1.1	1.5	<0.1	0.4	<0.1	**20**	**12**	2.2	7.3	0.7
Mn-oxides	1.7	1.4	**7.5**	**7.3**	**8.4**	**5.2**	1.6	**5.9**	2.8	0.9
Others	1.0	0.9	0.8	0.3	0.1	0.4	0.5	0.6	0.2	0.4
Other associations (%)										
Fe-oxides	**2.1**	1.7	**7.8**	**3.7**	**9.8**	1.7	1.3	1.1	0.7	0.4
Goethite	**4.0**	**4.7**	**4.9**	1.6	**4.2**	**2.9**	**2.8**	**7.4**	**3.5**	**5.8**
Quartz	0.3	**4.7**	0.2	0.3	0.1	1.8	0.1	**–**	0.5	**2.2**
Al-phosphates	**3.1**	**2.7**	**3.6**	**2.9**	**2.8**	2.7	2.8	0.4	**2.9**	**1.6**
Apatite	0.1	<0.1	–	–	–	0.1	0.3	**–**	<0.1	0.4
Gibbsite + kaolinite	0.2	0.1	3.5	0.1	2.2	1.4	0.1	**2.6**	–	–
Micas	<0.1	<0.1	0.1	0.1	0.1	–	–	**4.4**	–	–
Ilmenite	0.3	0.3	0.1	0.1	0.1	**2.9**	2.2	0.5	1.2	0.5
Ti-oxides	1.0	0.9	0.2	0.1	0.1	**6.9**	**5.0**	1.5	**2.0**	0.3
Perovskite	<0.1	–	–	–	–	0.9	0.1	–	–	–
Mn-oxides	1.1	1.0	2.8	**2.7**	5.2	1.6	1.2	2.9	1.2	0.3
Others	1.0	0.5	0.4	0.2	0.1	<0.1	0.7	0.3	1.0	0.2

netic separation of the Fe-oxy-hydroxides followed by flotation could be assessed, and a balance between energy for milling and recovery must be set. Otherwise, the chemical process must consider a pre-concentration to reduce the content of gangue minerals, such as Al-phosphates, Fe-oxy-hydroxides, Ti-minerals, mica, BaMn-oxy-hydroxides, and quartz, depending on the deposits (the main associations with the REMs).

Due to the complexity of REM occurrence and its relevance of resources, a multidisciplinary approach must be carried out to develop an integrated solution involving physical, chemical, and eventually biological methods, considering the costs, recovery, and other impacts.

Conflicts of interests

None declared.

Acknowledgements

The authors acknowledge the financial support of CNPq (National Council for Scientific and Technological Development, Brazil, Process 406923/2013-2) and the scholarships provided by CAPES (Coordination for the Improvement of Higher Education Personnel) to the researchers. They are also grateful to the anonymous reviewers, who greatly improved this manuscript, and to the Technological Characterization Laboratory (LCT-USP) from Universidade de São Paulo for providing the infrastructure.

REFERENCES

[1] BGS. Rare earth elements profile. British Geological Survey, 2011. 54p. http://www.bgs.ac.uk/ (accessed July 2016).
[2] USGS. Rare earths. Mineral Commodity Summaries – U.S. Geological Survey, 2019. pp. 132–3. http://minerals.usgs.gov/minerals/pubs/commodity/rare_earths/mcs-2019-raree.pdf (accessed March 2019).
[3] Massari S, Ruberti M. Rare earth elements as critical raw materials: focus on international markets and future strategies. Resour Policy 2013;38:36–43, http://dx.doi.org/10.1016/j.resourpol.2012.07.001.
[4] Golev A, Scott M, Erskine PD, Ali SH, Ballantyne GR. Rare earths supply chains: current status, constraints and opportunities. Resour Policy 2014;41:52–9, http://dx.doi.org/10.1016/j.resourpol.2014.03.004.
[5] MME. Plano Nacional de Mineração 2030 (PNM – 2030), Ministério das Minas e Energia – MME, Secretaria de Geologia, Mineração e Transformação Mineral – SGM, 2010. 157p. http://www.mme.gov.br/web/guest/secretarias/geologia-mineracao-e-transformacao-mineral/plano-nacional-de-mineracao-2030/pnm-2030 (accessed July 2016).

[6] Lima PCR. Terras-Raras: Elementos Estratégicos para o Brasil. Consultoria Legislativa. 2012. 266p. http://www2.camara.leg.br/a-camara/altosestudos/temas/temas-2013-2014/terras-raras/EstudoMineraisEstratgicoseTerrasRaras.pdf (Accessed July 2016).
[7] Rocio MAR, Silva MM, Carvalho PSL, Cardoso JGR. Terras-raras: situação atual e perspectivas. Mineração: BNDS Setorial, vol. 35; 2012. p. 369–420. http://www.bndes.gov.br/SiteBNDES/export/sites/default/bndes_pt/Galerias/Arquivos/conhecimento/bnset/set3511.pdf. (accessed July 2016).
[8] CGEE. Usos e aplicações de Terras Raras no Brasil: 2012–2030. Centro de Gestão de Estudos Estratégicos, 2013. 254p. http://www.cgee.org.br/publicacoes/terras_raras.php (accessed July 2016).
[9] Lapido-Loureiro FEV. O Brasil e a reglobalização da indústria das terras raras. Ministério da Ciência, Tecnologia e Inovação – MCTI, Centro de Tecnologia Mineral – CETEM; 2013, 204p.
[10] DNPM. Terras Raras. In Sumário Mineral 2015 (35) – Departamento Nacional de Produção Mineral. 2016, pp. 108–9. http://www.dnpm.gov.br/dnpm/sumarios/sumario-mineral-2015 (accessed July 2016).
[11] Biondi JC. Brazilian mineral deposits associated with alkaline and alkaline-carbonatite complexes. In: Comin-Chiaramonti P, Gomes CB, editors. Mesozoic to cenozoic alkaline magmatism in the Brazilian platform. 2005. p. 707–50.
[12] Tassinari MMML, Kahn K, Ratti G. Process mineralogy studies of Corrego do Garimpo REE ore, Catalao-I alkaline-complex, Goias, Brazil. Miner Eng 2001;14(12):1609–17, http://dx.doi.org/10.1016/S0892-6875(01)00179-0.
[13] Neumann R, Valarelli JV. Technological characterization of the potential RE ores from Córrego do Garimpo, Catalão, Central Brazil. J African Earth Sci 2001;32:A27, http://dx.doi.org/10.1016/S0899-5362(01)90054-5.
[14] Kahn H, Tassinari MMML, Ulsen C, Uliana D. Terras Raras – Monazita associada a complexos alcalino-carbonatíticos. Revista ABM Metalurgia, Materiais Mineração 2012;68:125–9.
[15] Antoniassi JL, Uliana D, Kahn H, Tassinari MMML, Ulsen C. Assessment and characterization of REE minerals from an alkali-carbonatitic complex. In: Dong F, editor. Proceedings of the 11th international congress for applied mineralogy – ICAM. 2015. p. 173–86, http://dx.doi.org/10.1007/978-3-319-13948-7.
[16] Neumann R, Medeiros EB. Comprehensive mineralogical and technological characterisation of the Araxá (SE Brazil) complex REE (Nb-P) ore, and the fate of its processing. Int J Miner Process 2015;144:1–10, http://dx.doi.org/10.1016/j.minpro.2015.08.009.
[17] Testa FG, Avelar AN, Silva RG, Souza CC. Caracterização mineralógica e alternativa para beneficiamento de litotipos mineralizados em terras raras do complexo alcalino de Catalão. Revista ABM Metalurgia Materiais & Mineração 2017;14:46–53, http://dx.doi.org/10.4322/2176-1523.1064.
[18] Gu Y. Automated scanning electron microscope based mineral liberation analysis – an introduction to JKMRC/FEI mineral liberation analyser. J Miner Mater Charact Eng 2003;2(1):33–41, http://dx.doi.org/10.4236/jmmce.2003.21003.
[19] Grammatikopoulos T, Mercer W, Gunning C. Mineralogical characterisation using QEMSCAN of the Nechalacho heavy rare earth metal deposit, Northwest Territories, Canada. Can Metall Q 2013;52(3):265–77, http://dx.doi.org/10.1179/1879139513Y.0000000090.
[20] Smythe DM, Lombard A, Coetzee LL. Rare earth element deportment studies utilising QEMSCAN technology. Miner Eng 2013;52:52–61, http://dx.doi.org/10.1016/j.mineng.2013.03.010.
[21] ISE. Institut für Seltene Erden und strategische Metalle. 2019. https://institut-seltene-erden.de/. (accessed September 2019).
[22] Berbert CO. Carbonatites and associated mineral deposits in Brazil. In Report of the Geological Survey of Japan – 263 1984:269–90.
[23] Mariano AN. Economic geology of rare earth minerals. In: Lipin BR, McKay GA, editors. Geochemistry and mineralogy of rare earth elements – 21. Reviews in mineralogy. 1989. p. 309–37.
[24] Waber N. The supergene thorium and rare-earth element deposit at Morro do Ferro, Poços de Caldas, Minas Gerais, Brazil. J Geochem Expl 1992;45:113–57, http://dx.doi.org/10.1016/0375-6742(92)90123-P.
[25] Kahn H, Sant'Agostino LM, Tassinari MMML, Ulsen C, Braz AB. Apatite from alkaline complexes – Behavior in mineral processing and characterization techniques. In: Zhang P, Swager K, Leal Filho L, El-Shall Org H, editors. Beneficiation of phosphates: technology advance and adoption. USA: SME – Society for Mining, Metallurgy and Exploration Inc.; 2010. p. 53–63.
[26] Soubiès F, Melfi AJ, Autefage F. Comportamento geoquímico dos elementos de terras raras nos alteritos da jazida de fosfato e titânio de Tapira (Minas Gerais, Brasil): a importância dos fosfatos. Revista Brasileira de Geociências 1991;21:1–16.
[27] Lapido-Loureiro FEV. Terras-Raras no Brasil: Depósitos, Recursos Identificados, Reservas. Centro de Tecnologia Mineral – CETEM; 1994, 189p.
[28] Oliveira SMB, Imbernon RAL. Weathering alteration and related REE concentration in the Catalão I carbonatite complex, central Brazil. J South Am Earth Sci 1998;11(4):379–88, http://dx.doi.org/10.1016/S0895-9811(98)00024-8.
[29] Barbosa ESR, Brod JA, Junqueira-Brod TC, Dantas EL, Cordeiro PFO, Gomide CS. Bebedourite from its type area (Salitre I complex): a key petrogenetic series in the Late-Cretaceous Alto Paranaíba kamafugite–carbonatite–phoscorite association, Central Brazil. Lithos 2012;144–145:56–72, http://dx.doi.org/10.1016/j.lithos.2012.04.013.
[30] Toledo MCM, Oliveira SMB, Fontan F, Ferrari VC, Parseval F. Mineralogia, Morfologia e Cristaloquímica da monazita de Catalão I (GO, Brasil). Revista Brasileira de Geociências 2004;34:135–46, http://dx.doi.org/10.25249/0375-7536.2004341135146.